

ATOMIC IMAGING OF OXYGEN DESORPTION FROM TUNGSTEN TRIOXIDE

A.K. PETFORD

Center for Solid State Science, Arizona State University, Tempe, Arizona 85287, USA

L.D. MARKS

*Department of Materials Science and Ipatiett Laboratories, The Technological Institute,
Northwestern University, Evanston, Illinois 60201, USA*

and

M. O'KEEFFE

Department of Chemistry, Arizona State University, Tempe, Arizona 85287, USA

We report direct observations by high-resolution electron microscopy of oxygen desorption from tungsten trioxide. Clear evidence is found for layer epitaxial growth of metallic tungsten with $(110)W \parallel (100)WO_3$ and $[001]W$ and $[001]WO_3$ parallel to the electron beam, consistent with low-energy electron diffraction data on the low-temperature epitaxy of WO_3 on W . $W[001]$ was always observed parallel to the electron beam independent of the surface normal. The results suggest that bulk and surface damage, and displacement processes, are similar.

1. Introduction

For the past few years electron- or photon-induced desorption processes have been studied with increasing interest. The processes can be classified under the general title “desorption induced by electronic transitions” (DIET) or “electron-stimulated desorption” (ESD). The original model put forward to explain desorption from surfaces was proposed by Menzel and Gomer [1] in 1964, and independently by Redhead [2] in the same year. This model could not adequately explain desorption results from ionically bonded surfaces, and in 1978, Knotek and Feibelman [3–5] proposed a new model based on Auger emission. The Knotek–Feibelman (K–F) mechanism applies primarily to maximal valence ionic solids – ones in which the metal ions effectively have no valence electrons. WO_3 is an example of such a material, with the tungsten ions in the noble-gas configuration W^{6+} , and the highest occupied tungsten orbitals sitting just below the Fermi level.

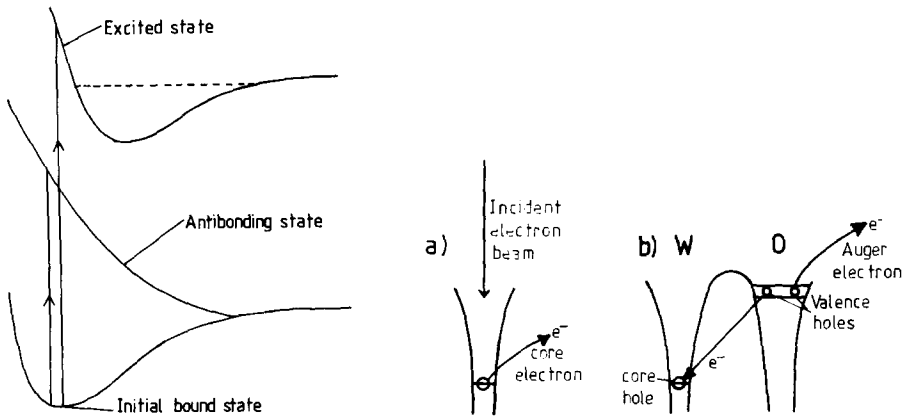


Fig. 1. Diagram illustrating the MGR mechanism. The inelastic excitation can be considered as a localized transition to either an antibonding level or an excited state above the bonding threshold.

Fig. 2. Diagram illustrating the Knotek–Feibelman model: (a) ejection of a core electron and (b) the interatomic Auger process.

The Menzel–Gomer–Redhead (MGR) mechanism considers a localized interband transition, in which an electron on the ion or neutral to be desorbed goes from a bonding state to an excited valence state which is either antibonding or above the dissociation level (see fig. 1). As originally conceived the K–F model proposes that a core hole created on a maximal valence ion (e.g. W^{6+}) by an incoming electron or photon decays by Auger emission. The only electrons available are on the anions (in this case the O^{2-} ions) and these are selectively stripped. A simple Auger process involves the loss of two electrons – one to fill the core hole on the cation and the second ejected as an Auger electron, resulting in the O^{2-} ion being converted to an O atom (see fig. 2). In a very small percentage of cases, two Auger electrons are emitted and an O^+ ion will be formed, but in both cases the oxygen will appear positively charged and will be repelled by Coulomb interaction with neighboring positive tungsten atoms and ejected from the surface. For further details on both mechanisms see refs. [6–8].

It has recently proved possible to study surfaces directly in projection, at the atomic level, by high-resolution electron microscopy (HREM) (e.g. refs. [9–11]) – a technique known as profile imaging. With careful choice of the operating conditions one obtains a faithful image of the atomic surface structure and even without these exact conditions one obtains a representative signal which can be interpreted with the aid of numerical image simulations. We report here results obtained using this technique to study WO_3 (preliminary reports of this work have been presented elsewhere [12,13]).

We were interested initially in seeing whether any relaxation or reconstruction occurred at the oxide surface. Instead, however, we observed a foreign layer at the surface which was identified as tungsten metal. The tungsten was observed to form a coherent epitaxial layer, the epitaxy being consistent with the known low-temperature epitaxy of WO_3 on W [14,15]. We know that we are using the electron microscope under conditions when we can expect electron-beam-induced damage in the bulk of the type known as ionization damage, e.g. refs. [16,17], and we are therefore able to strengthen the case suggested by many authors [5,8,18] that bulk and surface damage mechanisms are essentially the same.

2. Experimental techniques

Both bulk samples of WO_3 and WO_3 smoke particles were examined down an [001] zone (WO_3 has a slightly distorted cubic structure, but for convenience here we will use the idealized cubic cell with lattice parameter 3.7 Å). The bulk specimens were prepared by crushing under methanol and depositing the crushed WO_3 particles onto a holey carbon film on a copper grid. WO_3 smoke particles were prepared using a method similar to that used by Uyeda to

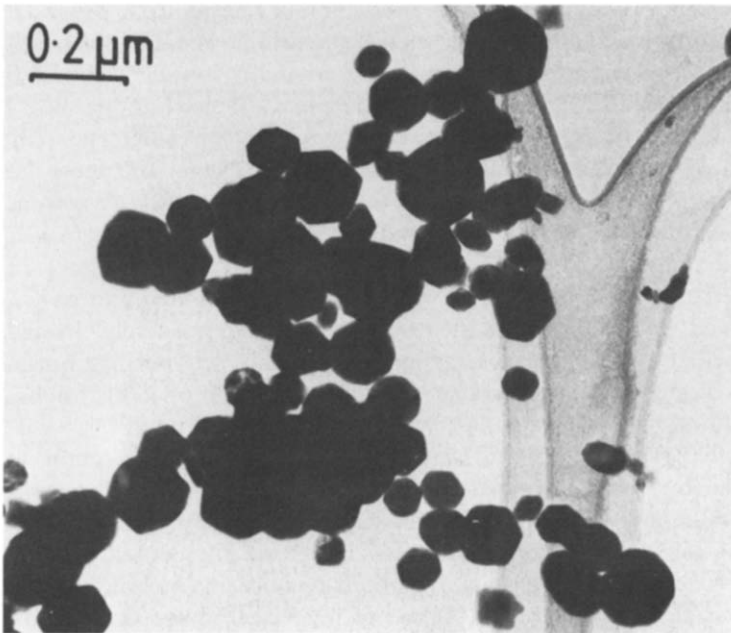


Fig. 3. Distribution of WO_3 smoke particles on a holey carbon film.

manufacture MgO particles [19]: a W-metal filament was heated in an evaporator under a low pressure of oxygen and the smoke particles produced were collected on a holey carbon film on a copper grid. A typical region of the carbon film showing the WO₃ smoke particle coverage is shown in fig. 3.

The WO₃ particles were examined in a 200 kV high-resolution electron microscope (JEOL 200CX). In order to ensure correct interpretation of experimental images, simulated images were calculated using programs employing the multislice technique [9]. The calculations were performed on a 512 × 256 array corresponding to a unit cell of dimensions 37 × 22.2 Å. The cell contained bulk oxide with a few layers of tungsten metal on two surfaces. The calculations were performed for the surface layers having the epitaxy relation WO₃(100) || W(110) with the beam direction along W[001] (|| WO₃[001]), that is: $10d_{110}(W) = 6d_{100}(WO_3)$, and $7d_{001}(W) = 6d_{001}(WO_3)$. 100 Å focal spread and 0.75 mrad convergence were included in the calculation by an incoherent sum to simulate the envelope terms.

3. Results

When the as-prepared specimens were examined, a carbonaceous contamination layer due to hydrocarbons in the atmosphere was observed in some cases on the surface of the particles. Exposure to a focused electron beam for ≈ 30 min etched this contamination layer away, leaving a clean oxide surface

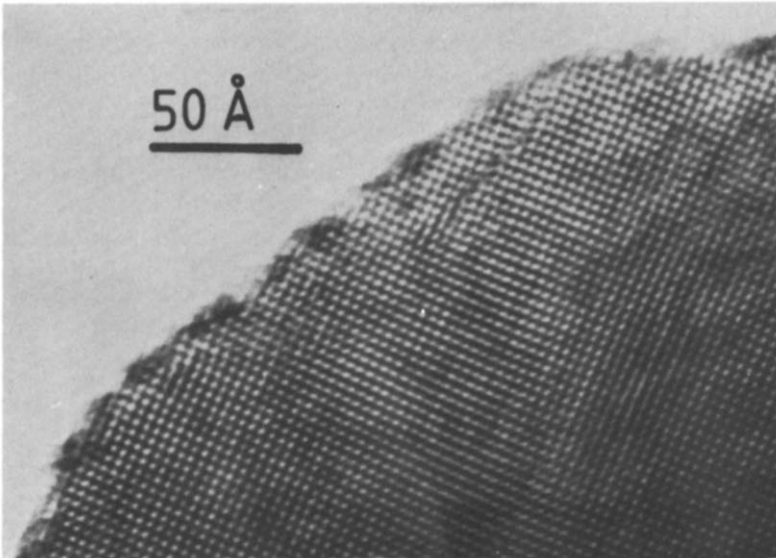


Fig. 4. HREM image of a WO₃ smoke particle. Crossed {100} fringes with $d = 3.7$ Å are visible.

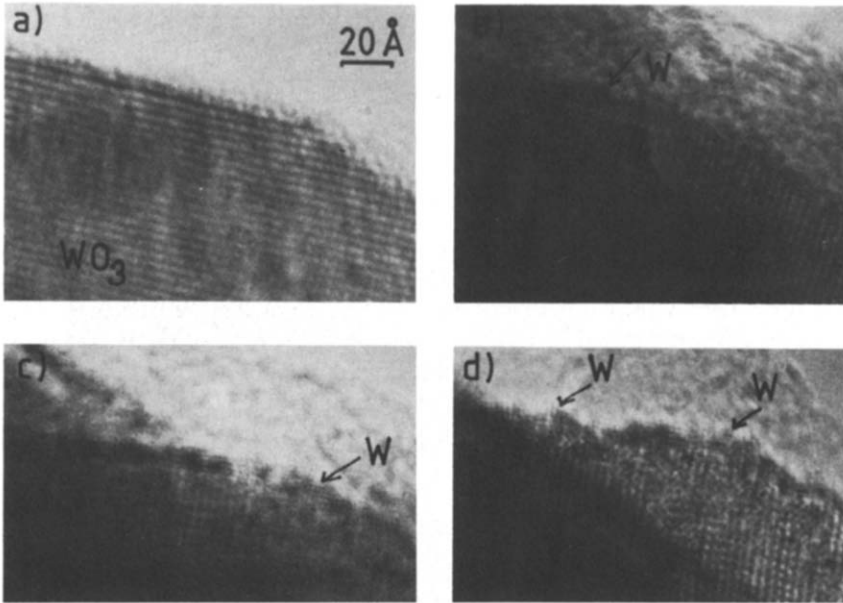


Fig. 5. Series of HREM images showing gradual growth of a W-metal layer on a WO_3 smoke particle. Images taken ≈ 30 min apart.

(see fig. 4). The etching of the carbonaceous layer is an electron-stimulated reaction due to water vapor in the microscope [10].

Further exposure to the beam of up to 3 h resulted in the slow growth of a surface layer of W metal on the WO_3 smoke particle, and also in the formation of some crystallographic shear planes in the bulk of the particle. The surface metal layer was initiated as small islands of metal which gradually grew (see fig. 5) until a thin continuous surface layer was seen (see fig. 6). In fig. 6a, 2.2 Å {110} fringes of tungsten metal are clearly visible in an epitaxial relationship with the 3.7 Å {100} tungsten trioxide fringes such that $(110)\text{W} \parallel (100)\text{WO}_3$, with $[001]\text{W}$ and $[001]\text{WO}_3$ parallel to the beam. A model of the epitaxy relation is shown in fig. 7, from which it is clear that it is essentially the same as the low-temperature epitaxy of WO_3 on W as determined by low-energy electron diffraction (LEED) [14,15]. The spacing of the fringes was measured accurately from the optical diffractograms shown in figs. 6b and 6c which were taken from the area imaged in fig. 6a. Diffractogram 6b is from the bulk of the WO_3 and shows only spots due to the WO_3 . Diffractogram 6c is from the surface and includes the tungsten metal layers and a few layers of WO_3 at the surface. The direction in which the diffractogram shows strong spots corresponds to the lattice repeat in the surface plane. The weak spots correspond to

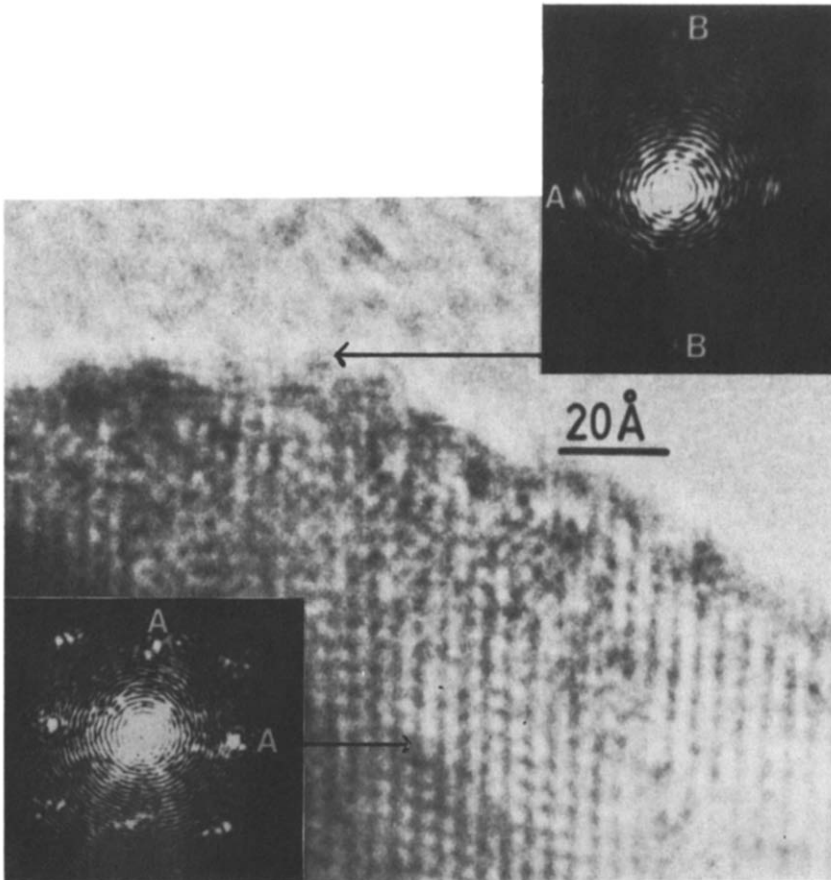


Fig. 6. (a) HREM image of a WO_3 smoke particle with a surface layer of W metal; 3.7 \AA $\{100\}$ fringes are visible in the WO_3 bulk and 2.2 \AA $\{110\}$ fringes in the surface W layer. (b) Optical diffractogram from WO_3 bulk, and (c) optical diffractogram from the surface layer. Spots labeled A are due to the 3.7 \AA spacing in WO_3 and those labeled B to the 2.2 \AA spacing in W.

the lattice repeat normal to the surface – only 2–3 lattice repeats are present in this direction.

The epitaxy $(110)\text{W} \parallel (100)\text{WO}_3$ was observed for at least 90% of the surfaces examined: this percentage may well be as high as 100% but the experimental evidence was not sufficiently clear cut for such a positive statement to be made. The epitaxy relation observed is illustrated in fig. 8. It is important to note that the structurally equivalent epitaxy with $[001]\text{W}$ normal to the beam was not observed, and that there was no evidence for any reduced oxides at the surface, confirming that the presence of W metal is not due to thermal

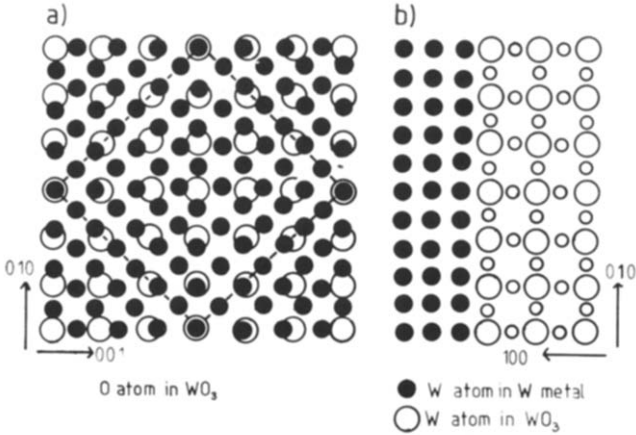


Fig. 7. Model for coincidence site epitaxy of W on WO₃: (a) normal to a (100) surface and (b) as seen in the experiment. Crystallographic directions refer to the WO₃ lattice.

reduction of the WO₃. (The reduced oxides would have been clearly distinguishable using the technique of HREM if present.)

Calculated images (see fig. 9) indicate that the tungsten metal fringes can be

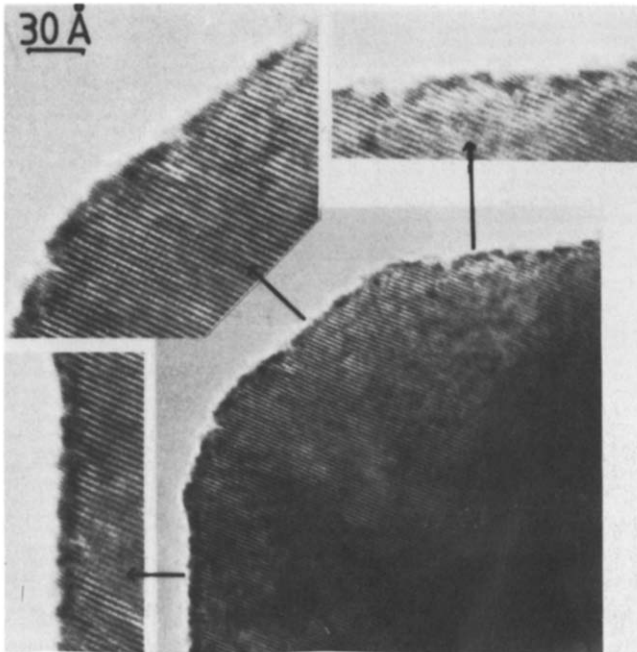


Fig. 8. HREM image of a WO₃ smoke particle with a surface W layer. The same epitaxy relation is seen on the different surfaces present.

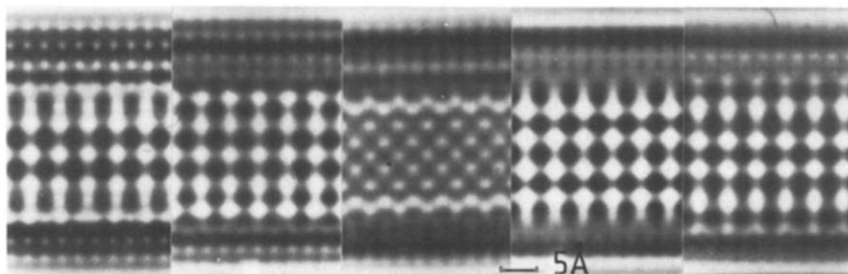


Fig. 9. Through focal series of calculated images at defocii (from left to right) of -1200 , -1000 , -800 , -600 and -400 Å. Specimen thickness is 31.7 Å. The top surface of the WO_3 has 3 layers of W and the bottom surface has 2 layers of W.

seen using the JEOL 200CX HREM but that a low focal spread and low beam convergence are necessary for them to be resolved clearly. Further calculations in which light atoms (carbon) were substituted for the surface layer of tungsten were carried out. These show that the surface layers cannot clearly be seen unless they are composed of heavy atoms (strong scatterers) as light atoms do not produce enough contrast. This excludes the possibility that we were observing a carbonaceous contamination layer. (It is in any case highly unlikely that contamination would form a crystalline layer with the 2.2 Å fringe spacings observed.)

Samples prepared from crushed bulk oxide crystals showed more tungsten coverage. In this case 10 – 20 Å of metallic tungsten is clearly visible on the oxide surface, and again no reduced oxides were present (see fig. 10). It is not obvious to us why a thicker layer of W metal should grow on the bulk oxide crystals than on the WO_3 smoke particles: this effect could be due to impurities in the WO_3 bulk or to the imperfect surface of the bulk oxide

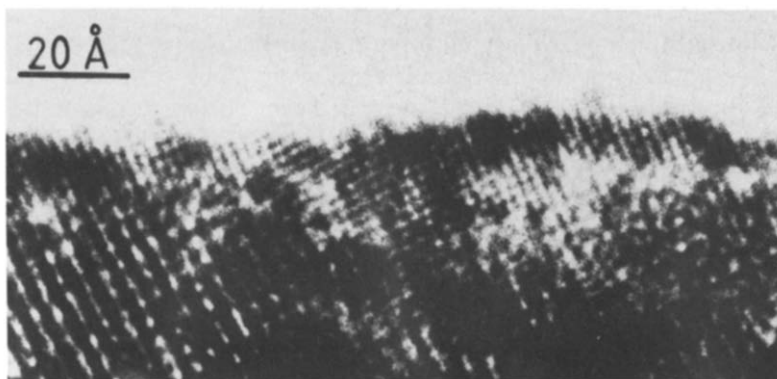


Fig. 10. HREM image of crushed bulk crystal specimen of WO_3 . A thick epitaxial layer of W metal is present.

particles. Alternatively, if one examines fig. 10, it is clear that the surface of the WO_3 is faceted such that it consists of a number of small (100) surfaces. This may aid the production of a thicker metal layer: at the outermost corner of a facet, fewer layers of W metal form, providing an easy path for the loss of further oxygen atoms due to desorption.

Two further points are worth noting here (also for the case of bulk oxide crystals) – firstly, during exposure to the electron beam a number of crystallographic shear planes formed perpendicular to the surface. Secondly, if one measures the lattice spacings of the (100) WO_3 planes perpendicular to the crystal surface, it can be seen that the interface mismatch strain has been accommodated primarily by the WO_3 rather than by the surface metal layer – the opposite effect to that normally observed at an interface between a bulk material and a surface layer.

4. Electron-stimulated desorption

It is appropriate here to compare the type of processes important in ESD for high-energy electrons with those for low-energy electrons: energy-loss processes for fast electrons are well established, e.g. refs. [20,21]. The primary excitations are phonons, plasmons, single-electron, interband and core excitations. Of these, phonons (leading to heating) typically occur for energies of 10^{-1} – 10^{-2} eV. WO_3 is a poor thermal conductor, and the thermal decomposition of WO_3 would be expected to lead to non-stoichiometric WO_{3-x} , e.g. ref. [22]. Reduced oxides of this type were not observed experimentally at the surface. We feel that high-energy processes such as inner-shell excitations in the target (> 1 keV) are unlikely as the cross sections are very small, and therefore only energy-loss processes in the range 5–100 eV, namely plasmon, interband, single-electron and low-energy core-loss processes will be considered.

The slow rate at which the oxygen desorption occurs is to be expected; well beyond the threshold energy of a process the cross section for a core-excitation process is inversely proportional to the incident beam energy, being of the order of 10^3 times smaller at 200 kV than at typical low-energy electron diffraction (LEED) energies, so that although in an electron microscope the beam density is typically 10^2 to 10^3 times that in most LEED experiments, most of this increased electron density is compensated for by the reduced scattering probability. Furthermore, essentially all the fast electrons ($> 99.9\%$) are transmitted through a thin (≈ 100 nm) specimen, whereas many of the 1 keV electrons incident upon a bulk specimen are completely stopped, producing a substantial secondary shower (which can itself lead to ESD). For further details and references on the inelastic processes for fast electrons see Raether [20] and Otsuki [21], and for the specific case of surfaces see Howie [23].

In a generalized case, the process occurs in three stages:

- (1) The fast electron initiates a change in the target electronic structure. The fast electron passes the target atoms in $\approx 10^{-19}$ s, a time too short for the target electrons to respond; momentum is transferred in an inelastic process, but there is insufficient time for any change in the configuration of the target electrons.
- (2) The target electrons are excited leading to a change in atomic potential (this occurs in $\approx 10^{-16}$ s).
- (3) The change in potential of the excited atom is a perturbation which acts as a driving force, leading to desorption in $\approx 10^{-12}$ s [24].

For the case of a high-energy incident electron undergoing an inelastic scattering process for which the energy loss is in the range 5–100 eV the momentum transfer is almost entirely perpendicular to the beam (from momentum and energy conservation) [25]. The excited tungsten core electron will not necessarily leave the tungsten atom immediately, but can remain in an extended distorted orbit. Thus, if the desorption process is governed by the final state of the tungsten atom, the anisotropy of the momentum transfer will lead to an anisotropy in the desorption, which will occur primarily normal to the beam direction. In contrast, if the desorption depends on the emptied core state, there will probably be a minimal anisotropy effect. The change in the electronic potential, which is believed to drive the desorption process [24], will look rather like the planet Saturn: a central core hole surrounded by a disc due to the ejected electron.

For a given tungsten atom, there are 3 possible oxygens which can donate an electron and be desorbed; it is of interest to note that the angle at which oxygen ions or neutrals are desorbed from a WO_3 surface has been measured experimentally [26] and it was observed that the oxygens are emitted in narrow cones around the direction of the bond between the desorbed oxygen and the tungsten atom to which it has donated an electron. We suggest that the direction of momentum transfer in the initial core excitation could affect the subsequent oxygen desorption, leading to desorption of the oxygen with the W–O bond parallel to the momentum transfer direction. For example, in the case of WO_3 , if the initial momentum transfer process by which the oxygen ion loses electrons occurs in the image plane, the subsequent oxygen ejection will occur in the same plane. It should be noted that we have not carried out a detailed analysis of the magnitude of the momentum transfer, and until this is done we cannot be sure that the effect is large enough to influence the oxygen desorption direction. Obviously a more detailed theoretical study is needed.

The direction of oxygen loss may subsequently affect the epitaxy observed. This could explain the experimentally observed dependence of the epitaxy on the beam direction, although there are other possible reasons. The tungsten atoms initially freed from the oxide may be expected to have some mobility so that it is also possible that they order into an arrangement of lowest interfacial

energy (as seen in fig. 7a). The fact that only one of two structurally equivalent epitaxies is observed further suggests that this ordering is influenced by the direction of the electron beam. Examination of fig. 7a shows that the observed layer of W on WO₃ has the lowest possible density of atoms in a projection along the beam direction.

5. Discussion

Perhaps the most significant aspect of our results is its implications in the general area of radiation effects, both at surfaces and in the bulk. We can expand our discussion here to include electron-stimulated reactions (i.e. chemical reactions) (ESR) as well as desorption; an example of an electron-stimulated reaction is that of carbon with water vapor [10] which we have made use of in some cases to clean the WO₃ particle surfaces. We suspect that all electron-stimulated phenomena have similar initial processes, but differ in the particular channel of the final decay. We are not alone in this view – see for instance refs. [5,8,18]. We also feel that ESD and ESR will both occur under the *same* conditions as bulk ionization damage (ionization damage is the name given to any process whose cross section shows an inverse dependence on the incident electron beam energy, as against ballistic knock-on phenomena which have typical threshold energies 100–1000 keV). For example the Knotek–Feibelman Auger decay mechanism may well describe the initial excitation process leading to bulk radiation damage in WO₃: an oxygen neutral produced by such a process may not be able to escape to the surface, but could move through the lattice to an interstitial site – forming a Frenkel defect within the bulk of the material.

In fact the currently accepted mechanisms for ionization damage are very similar to those for ESD. The MGR process is very similar to the Pooley–Hersh mechanism [25,26], whilst core excitation was first suggested in bulk materials by Varley [27]. We can expect MGR phenomena to be substantially faster than K–F processes (in an electron microscope) since interband excitations are noticeably stronger than core excitations. This assumes that the efficiency of the MGR and K–F mechanisms is the same, although the K–F mechanism is probably more efficient in this case. In materials such as the alkali halides and organic specimens when some form of MGR process is presumably occurring, severe damage occurs on a time scale of minutes or even seconds under our experimental conditions. This contrasts with our observation of a K–F process in which desorption occurs on the order of a monolayer every 30 min.

A few examples of electron-microscopy observations of ESD and ESR can be given here (although they have not necessarily been recognized as such): the observation by Iijima [28] of a metal overlay, probably aluminium, on the surface of γ -alumina particles; the drilling of small holes in materials such as

Al₂O₃ and MgO using an intense electron beam, observed by Salisbury [29], and the observation of niobium at the surface of titanium niobium oxide [30]. Similar processes probably occur in electron-beam-induced sublimation of many oxides. An example is that of MgO which sublimes in an intense electron beam; here we expect ESD of the oxygen followed by evaporation of the volatile magnesium.

The main differences between processes in the bulk and at a surface are probably due to the different steric hinderance. Here it seems best to use the term electron-stimulated displacement. In the bulk it will be harder to move an atom into an interstitial site because of the hard core repulsion of the surrounding cage of atoms. There are some indications in our results that the metallic tungsten layers inhibit further oxygen loss when 2–3 monolayers thick.

As a final point, it is worthwhile to emphasize that our results suggest that one may, with care, be able to observe adsorbates on surfaces directly using the profile imaging technique. The higher beam densities present in an HREM are offset by the reduced scattering probabilities and the substantially smaller secondary shower at higher voltages. Minimum-exposure techniques, such as those used for imaging biological specimens, may well prove viable.

Acknowledgements

This research was supported by the Facility for High Resolution Electron Microscopy, in the Center for Solid State Science at Arizona State University, established with support from the National Science Foundation (Grant DMR-8306501). This research was funded on NSF Grant DMR-8418083 (A.K. Petford and M. O'Keeffe) and by the University Research Grants Committee at Northwestern University (L.D. Marks).

References

- [1] D. Menzel and R. Gomer, *J. Chem. Phys.* 40 (1964) 1164.
- [2] P.A. Redhead, *Can. J. Phys.* 42 (1964) 886.
- [3] M.L. Knotek and P.J. Feibelman, *Phys. Rev. Letters* 40 (1978) 964.
- [4] P.J. Feibelman and M.L. Knotek, *Phys. Rev.* B18 (1978) 6531.
- [5] M.L. Knotek and P.J. Feibelman, *Surface Sci.* 90 (1979) 78.
- [6] Articles in: *Desorption Induced by Electronic Transitions, DIET 1*, Eds. N.H. Tolk, M.M. Traum, J.C. Tully and T.E. Madley (Springer, Berlin, 1983).
- [7] M.L. Knotek, *Phys. Scripta* T6 (1983) 94.
- [8] M.L. Knotek, *Phys. Today*, September 1984, p. 27.
- [9] L.D. Marks, *Surface Sci.* 139 (1984) 1000.
- [10] L.D. Marks and D.J. Smith, *Surface Sci.* 143 (1984) 495.
- [11] D.J. Smith and L.D. Marks, *Ultramicroscopy* 16 (1985) 101.
- [12] L.D. Marks, A.K. Petford and M. O'Keeffe, *Nature*, submitted.

- [13] L.D. Marks, A.K. Petford and M. O'Keeffe, Proc. 43rd Ann. EMSA Meeting, Louisville, 1985, p. 266.
- [14] N.R. Avery, Surface Sci. 41 (1974) 533.
- [15] E. Bauer and T. Engel, Surface Sci. 71 (1979) 695.
- [16] N. Itoh, Radiation Effects 64 (1982) 161.
- [17] L.W. Hobbs, in: Introduction to Analytical Electron Microscopy, Eds. J.J. Hren, J.I. Goldstein and D.C. Joy (Plenum, New York, 1979) p. 437.
- [18] See in particular D.E. Ramaker in ref. [6], p. 70.
- [19] T. Ohno, S. Yatsuya and R. Uyeda, Japan. J. Appl. Phys. 15 (1976) 1213.
- [20] H. Raether, Excitation of Plasmons and Interband Transitions by Electrons (Springer, Berlin, 1980).
- [21] Y.H. Otsuki, Charged Beam Interaction with Solids (Taylor and Francis, Philadelphia, 1983).
- [22] L.A. Bursill, J. Solid State Chem. 48 (1983) 256.
- [23] A. Howie, Ultramicroscopy 11 (1983) 141.
- [24] J.W. Gadzuk in ref. [6], p. 4.
- [25] D. Pooley, Solid State Commun. 3 (1965) 241.
- [26] H.N. Hersh, Phys. Rev. 148 (1966) 928.
- [27] J.H.O. Varley, Nature 174 (1954) 886; J. Nucl. Energy 1 (1954) 130.
- [28] S. Iijima, Japan. J. Appl. Phys. 23 (1984) L347.
- [29] I.G. Salisbury, R.S. Timsit, S.D. Berger and C.J. Humphreys, Appl. Phys. Letters 45 (1984) 1289.
- [30] D.J. Smith, L.A. Bursill, L.D. Marks and P.J. Lin, Proc. 43rd Ann. EMSA Meeting, Louisville, 1985, p. 256.